Journal of the Mechanical Behavior of Biomedical Materials 100 (2019) 103368

Contents lists available at ScienceDirect

Journal of the Mechanical Behavior of Biomedical Materials

journal homepage: www.elsevier.com/locate/jmbbm

The effect of blast overpressure on the mechanical properties of the human tympanic membrane

Junfeng Liang[a,b], Kyle D. Smith[b], Rong Z. Gan[b], Hongbing Lu[a,*]

[a] Department of Mechanical Engineering, The University of Texas at Dallas, Richardson, TX, 75080, USA
[b] School of Aerospace and Mechanical Engineering, University of Oklahoma, Norman, OK, 73019, USA

ARTICLE INFO

Keywords:
Hearing damage
Blast overpressure
Tympanic membrane
Micro-fringe projection
Mechanical properties

ABSTRACT

The rupture of the tympanic membrane (TM) is one of the major indicators for blast injuries due to the vulnerability of TM under exposure to blast overpressure. The mechanical properties of the human TM exhibit a significant change after it is exposed to such a high intensity blast. To date, the published data were obtained from measurement on TM strips cut from a TM following an exposure to blast overpressure. The dissection of a TM for preparation of strip samples can induce secondary damage to the TM and thus potentially lead to data not representative of the blast damage. In this paper, we conduct mechanical testing on the full TM in a human temporal bone. A bulging experiment on the entire TM is carried out on each sample prepared from a temporal bone following the exposure to blast three times at a pressure level slightly below the TM rupture threshold. Using a micro-fringe projection method, the volume displacement is obtained as a function of pressure, and their relationship is modeled in the finite element analysis to determine the mechanical properties of the post-blast human TMs, the results of which are compared with the control TMs without an exposure to the blast. It is found that Young's modulus of human TM decreases by approximately 20% after exposure to multiple blast waves. The results can be used in the human ear simulation models to assist the understanding of the effect of blast overpressure on hearing loss.

1. Introduction

Blast-induced injuries commonly occur under such situations as accidents on construction sites and during terrorist attacks and military conflicts where the explosion takes place (Owens et al., 2008; Wolf et al., 2009). In explosion, the massive explosive energy released often leads to four types of injuries: primary, secondary, tertiary, and quaternary blast injuries. The primary injury is caused by the direct impact of the over-pressurized wave, in the form of rupture of gas-filled organs including lungs, middle ear, and eyes. The secondary injury results from flying debris and bomb fragments and occurs on the surface of a victim. The tertiary injury includes limb fracture, brain injury, and body part injury caused by blunt impact when an individual is thrown away by the blast wind. All the other explosion-related injuries especially those illnesses and diseases exacerbated by the blast are referred to as the quaternary injuries; they may include the exacerbation of asthma from toxic smoke and hyperglycemia from the trauma. The primary blast injury is often given the greatest concern (Mathews and Koyfman, 2015; Nakagawa et al., 2011).

Hearing loss or auditory system damage is one of the most critical sequelae among the primary blast injuries. As an air-filled organ, the ear is one of the most vulnerable organs to blast overpressure. Blast-induced hearing injury is categorized into tympanic membrane (TM) perforation or rupture, middle ear ossicular disruption, cochlear hair cell loss, and rupture of round window (Yeh and Schecter, 2012). The TMs have the lowest pressure threshold for injury in the auditory system; hence rupture of the human TM is one of the most common primary blast injuries. As an example, in the 2013 Boston blast, 90% of the hospitalized patients experienced TM perforation (Remenschneider et al., 2014). Because the lesion of the TM is strongly associated with hearing loss and tinnitus, the rupture of TM is usually a marker or an indicator for primary blast injury (Dougherty et al., 2013). The TM is a viscoelastic material with mechanical properties changing significantly at high frequencies or high strain rates (Luo et al., 2009). Even before the overpressure reaches the rupture threshold, it may have already experienced loading pressure at a high strain rate. This overpressure can potentially induce sub-microscopic damage to the fiber layers of the TM, which is difficult to observe directly, but can be severe enough to

* Corresponding author. Department of Mechanical Engineering, University of Texas at Dallas, 800 W Campbell Rd, ECSN 2.528, Richardson, TX, 75080-3021, USA.

E-mail address: hongbing.lu@utdallas.edu (H. Lu).

https://doi.org/10.1016/j.jmbbm.2019.07.026
Received 21 March 2019; Received in revised form 14 June 2019; Accepted 22 July 2019
Available online 07 August 2019

alter the overall mechanical properties of the TM (Engles et al., 2017; Liang et al., 2017).

Recently, using a miniature split Hopkinson tension bar, Luo et al. (2016) determined that the Young's modulus of the human TM at different strain rates changes significantly after its exposure to blast overpressure. Engles et al. (2017) measured the dynamic properties of the strips cut from blast-exposed TMs using acoustic loading and a laser Doppler vibrometer (LDV). They also found that both storage and loss moduli of the TM exhibit pronounced decrease over a frequency range of 200–8000 Hz. However, in those studies, strip specimens cut from the TM were used; cutting a TM into strips may alter the physiological condition of the TM (O'Connor et al., 2008). To circumvent this issue, a micro-fringe projection technique was used for characterization of the mechanical properties for chinchilla TMs (Liang et al., 2017). In this bulging experiment, fringes with sub-millimeter pitch are projected onto the TM, and quasi-static air pressure is applied to the TM. A comparison between control and post-blast chinchilla TMs shows that there is about a 50% reduction in Young's modulus for the post-blast chinchilla TM. The decrease is larger than that of a human TM observed by Engles et al. (2017) and Luo et al. (2016).

In this paper, we apply the micro-fringe projection technique on the human TMs to evaluate the change of the mechanical properties of the human TM after its exposure to the blast overpressure. The intact, full-size TMs in human cadaver temporal bones are used directly without sectioning in bulging experiments. They are subjected to multiple exposures of blast waves with a pressure slightly lower than the rupture threshold (~70 kPa) of the human TM (Gan et al., 2018). Results are compared between the control (normal) and post-blast TMs to evaluate the role of blast over-pressure on the mechanical property change of the human TMs.

2. Methods

2.1. Exposure of the human TMs to blast waves

Fresh human cadaveric temporal bones (n = 16) containing the intact auditory system from the Life Legacy Foundation, a certified human tissue supplier for military research, are used in this study. The protocol has been approved by the U.S. Army Medical Research and Material Command (USAMRMC) Office of Research Protections (ORP). To prepare the post-blast TM sample, the temporal bone is mounted to a head block placed inside a blast chamber where it is exposed to blast overpressure. The experiment is conducted in the Biomedical Engineering Laboratory at the University of Oklahoma (Fig. 1). The blast overpressure is generated using a composessed-nitrogen-driven blast apparatus. A 130-μm thick polycarbonate film is used as a diaphragm sealing the outlet of the blast apparatus, the rupture of which releases blast overpressure between 45 and 55 kPa. The magnitude of overpressure applied on a TM is controlled by varying the distance between the blast outlet and the TM, and monitored by a pressure sensor (Model 102B16, PCB Piezotronics, Depew, NY) located at the entrance of the ear canal (approximately 1 cm from the ear canal opening). A data acquisition system using a LabVIEW interface on a PC (cDAQ 7194 and A/D converter 9215, National Instruments Inc., Austin, TX) with a sampling rate of 100 kS/s (10-μs interval) is used to acquire the pressure data. For the purpose of comparison, five control TMs (which are not exposed to blast waves) are harvested as the control TM samples prior to the TM blast experiments. The TM sample information is shown in Table 1. The remaining temporal bones are exposed to three times of blast with an average peak pressure of 50 kPa (equivalent to a sine wave of 188 dB SPL), which is below the rupture threshold of the human TM (~70 kPa). The information for this group of TM samples is listed in Table 2.

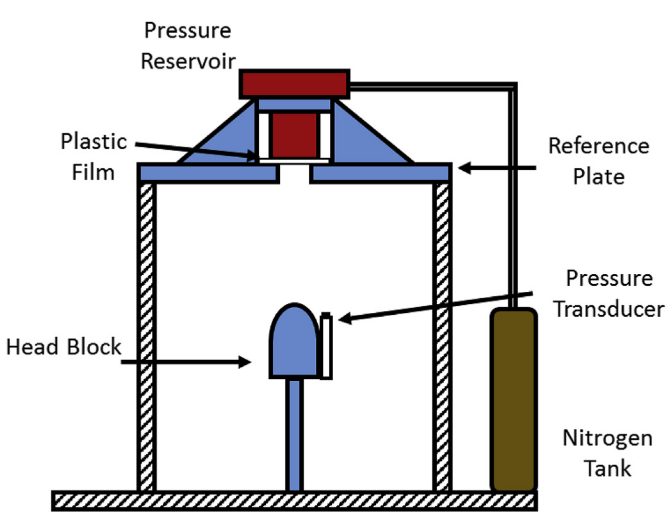

Fig. 1. Schematic of the blast testing chamber and the sample setup. For demonstration purposes, the components are not drawn to scale.

2.2. Sample preparation

To prepare a sample for the micro-fringe projection measurement, each temporal bone is first trimmed to a small bony block containing the entire TM and the entire middle ear. Then the ear canal is carefully ground until the TM is fully exposed. A 3-mm diameter hole is drilled in the posterior-superior area of the middle ear and a polyvinyl chloride (PVC) tubing (1.5 mm inner diameter, 3 mm outer diameter, 75 mm long) is inserted into the hole and sealed on the bony block with "two-part epoxy" (Devcon and 5 Minute, Illinois Tool Works Inc). The outer surface of the entire bony block is further sealed with paraffin to keep the middle ear cavity in an airtight condition. After the epoxy is fully cured, the outer end of the tubing is connected to a pressure monitoring system that consists of a syringe pump and a pressure gauge to apply static pressure to the TM from the medial side (Fig. 2). The time it takes to prepare a temporal bone before the measurement is approximately 45 min. To protect the TM from dehydration, a droplet of 0.9% saline solution is applied to the TM at 5-min intervals during the measurement. Meanwhile, the TM is covered with paper saturated with saline solution during the curing of the epoxy. To produce high-quality TM fringe images, the lateral surface of the TM is coated with a thin layer of titanium oxide (100 mg/ml) in saline to provide a diffused reflective surface. Titanium oxide has been widely used in Moiré techniques to measure the TM motion. A thin layer of titanium oxide coating is not anticipated to affect the mechanical response of the TM (Liang et al., 2015, 2016, 2017; Dirckx and Decraemer, 1997).

2.3. Micro-fringe projection experiments

A micro-fringe projection system is used to measure the volume displacement of the TM under different static pressures coupled with a 3-dimensional surface reconstruction algorithm. The system consists of a micro-fringe projector, a surgical microscope (Zeiss, model 50881) and a digital camera (Nikon D7000) as shown in the schematic diagram in Fig. 3. The micro-fringe projector projects the shadow of a fine Ronchi ruling grating with pitch density of 20 cycles/mm (Edmund Optics) onto the TM surface using a fiber optic illuminator (Techniquip Corp. model R150-A2). Stepwise pressures with increments of ± 0.125 kPa up to ± 1.0 kPa are applied through a PVC tube onto the middle ear side of the bony block and monitored with a pressure gauge. Images of the fringe patterns on the TM under different pressures are acquired with the Nikon digital camera connected to the surgical microscope. Before each test, the TM is preconditioned by applying a small pressure with a magnitude of 100 Pa for five cycles. This allows the tissue material to reach a steady state (Liang et al., 2016; Gaihede, 1996). Virtual interferometry is formed by digitally combining the

Table 1
Dimensions and parameters of the Ogden model for each control human TM.

Sample Number	Superior-Inferior Diameter (mm)	Anterior-Posterior Diameter (mm)	μ_1 (MPa)	α_1	μ_2 (MPa)	α_2
TB15-51	8.94	9.62	4.2	3.0	-1.3	0.8
TB15-52	7.81	8.89	3.7	3.2	-1.2	0.8
TB16-11	7.09	9.12	4.3	2.7	-1.0	0.8
TB16-12	8.53	8.91	3.8	2.6	-1.3	0.9
TB16-19L	7.95	8.12	4.1	2.6	-1.1	0.9
Average ± Standard Deviation	8.06 ± 0.63	8.93 ± 0.48	4.0 ± 0.2	2.8 ± 0.2	-1.2 ± 0.1	0.8 ± 0.1

Table 2
Dimensions, average pressure for the blast wave and parameters of the Ogden model for each post-blast human TM.

Sample Number	Superior-Inferior Diameter (mm)	Anterior-Posterior Diameter (mm)	Average Blast Pressure (kPa)	μ_1 (MPa)	α_1	μ_2 (MPa)	α_2
TB15-59	8.57	7.90	48	3.8	3.1	-1.5	1.0
TB15-60	8.83	7.77	48	3.7	3.0	-1.1	1.0
TB15-63	7.54	7.90	48	3.5	2.8	-1.5	1.0
TB15-64	7.43	7.04	48	3.6	2.9	-1.5	0.9
TB16-47	8.55	6.91	46	3.4	2.7	-1.2	0.9
TB16-48	8.24	7.15	46	3.5	3.0	-1.5	1.2
TB16-1L	10.0	7.12	61	4.0	2.4	-1.5	0.9
TB16-2R	8.53	6.95	61	3.3	2.8	-1.5	0.9
TB14-19	8.11	8.10	52	3.5	2.5	-1.1	1.0
TB14-20	8.55	7.89	45	3.9	2.6	-1.4	1.0
TB17-2R	10.7	10.3	26	2.4	-1	0.9	3.8
TB17-7L	8.5	8.3	28	2.1	-1.1	0.8	4.0
TB17-8R	9.6	7.2	25	2.4	-1.4	0.9	3.6
TB17-9L	9.9	7.8	21	2.7	-1.4	1.1	3.1
TB17-10R	7.7	7.7	26	2.8	-1.4	0.9	3.7
TB17-2R	8.3	7.2	26	2.4	-1	0.9	3.8
Average ± Standard Deviation	8.69 ± 0.89	7.68 ± 0.80	32 ± 13	3.6 ± 0.6	2.8 ± 1.9	-1.4 ± 1.1	1.0 ± 1.3

fringe pattern projected onto the TM with a reference fringe pattern projected onto a flat plane. Topography of the human TM that contains the height information of the TM surface is reconstructed from the interferometry using software Joshua (developed by Manuel Heredia at University of Sheffield) based on a five-step phase-shifted algorithm (Ortiz and Patterson, 2005). The resolution of the topography depends on the fringe density and the camera resolution. For the system used in this study, the height resolution is ~15 μm (Liang, 2009). To quantify the deformation of the TM under different static pressures, volume displacements are calculated by subtracting the reconstructed surface topography of the TM under pressure with that of the TM at the zero-pressure state. Details on the calculation of the surface topography and volume displacement calculations are described in previous publications (Liang et al., 2015, 2016, 2017).

2.4. Finite element method analysis

A finite element method (FEM) model for the human TM is established based on the surface topography of a human TM at the zero-pressure state reconstructed from the micro-fringe projection. The surface topography is converted to a three-dimensional solid model by computer-aided design (CAD) software (SolidWorks, 2014) and then further meshed into a FEM model for simulations in ANSYS15.0. Because the TM thickness is small compared to its major or minor axis, the TM is modeled as a shell with a thickness of 80 μm according to the average thickness of the human TMs used in this study. To match the model results with the experimental data, the dimensions of the TM FEM model are modified to appropriately reflect those of each individual TM sample. The dimensions of the TM samples used for

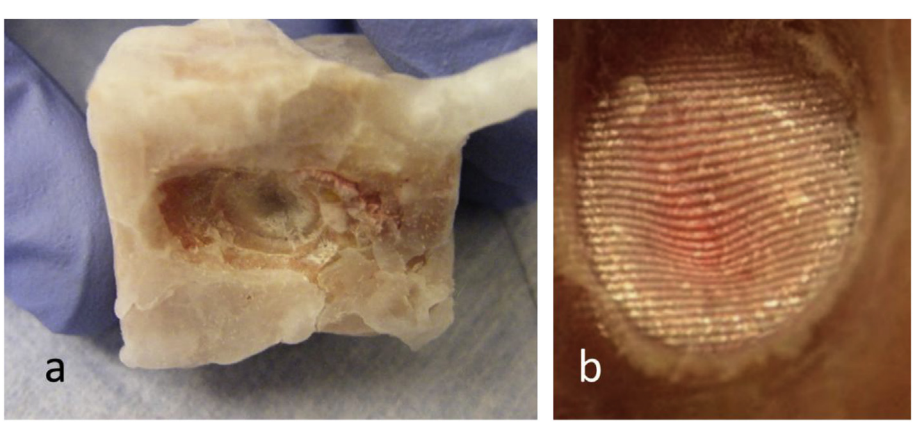

Fig. 2. Sample preparation: a) the bony block containing the entire middle and inner ear sealed with paraffin b) the human TM painted with titanium oxide.

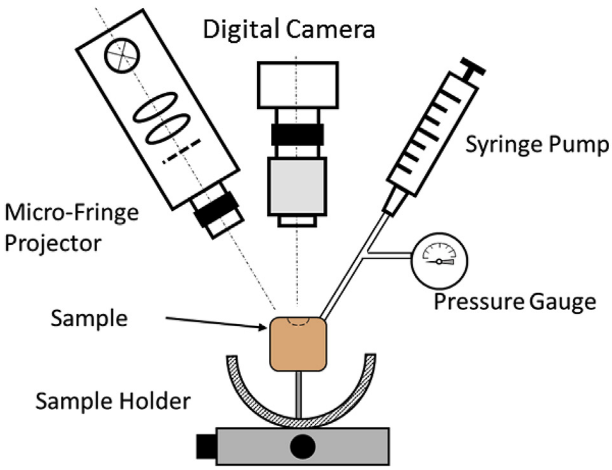

Fig. 3. Schematic view of the micro-fringe projection system and the pressure monitoring system utilized in this study.

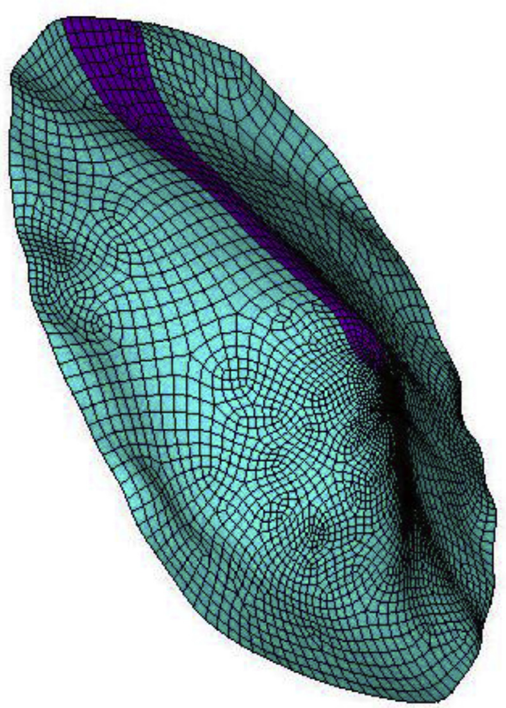

Fig. 4. Finite element mesh for TB15-51. The purple area is the simplified manubrium.

adjusting the FEM models are listed in Tables 1 and 2. To simplify the model, the manubrium of the malleus attached to the TM is also simulated as a section of the shell model of the TM using the properties of bone (10 GPa Young's modulus and 0.2 Poisson's ratio). The annulus of the TM is fixed for all degrees of freedom (no translation or rotation). The entire model (including the membrane and the manubrium) contains ~10,000 4-node tetrahedral shell elements (shell-181). Uniform pressures with an increment of ± 0.125 kPa up to ± 1.0 kPa are applied on the medial side of the TM. The boundary conditions, loading, and meshes of the TM FEM model are shown in Fig. 4. For each individual TM sample, the simulated volume displacement is calculated under each static pressure. It is noted that the actual connection between manubrium and TM is complicated and varies among individuals. Between the umbo and the lateral process of the malleus, the TM and the manubrium are connected through a layer of soft tissue (De Greef et al., 2016). To evaluate the effect of the coupling of the TM and the manubrium on the TM displacement in our model, a testing simulation is conducted. According to the results from De Greef et al., 25% of the length of the manubrium around the umbo and 12.5% of the length of the manubrium around the lateral process are set to have the properties of the bone. The remaining part of the manubrium is set to have the mechanical properties of the TM. The simulation results under 1 kPa show that the volume displacement changes only by 3.8%. Thus the variation of the TM-manubrium connection does not have a significant effect on our simulation results.

Similar to the studies on guinea pigs and chinchillas (Liang et al., 2015, 2016, 2017), the 2nd-order Ogden model is used in this study to describe the mechanical behavior of human TM under large deformations. The uniaxial form of the 2nd-order Ogden model is given as (Aernouts et al., 2010; Wang et al., 2002).

$$T_U = \sum_{i=1}^{2} \frac{2\mu_i}{\alpha_i}\left(\lambda_U^{\alpha_i - 1} - \lambda_U^{-0.5\alpha_i - 1}\right) \tag{1}$$

where T_U is the uniaxial stress; λ_U is the uniaxial stretch ratio, and $\lambda_U = 1 + \varepsilon_U$, with ε_U being the uniaxial strain. The parameters μ_i and α_i are constants representing the material hyperelastic properties. Under uniaxial stretch, assuming incompressibility of the TM, the principal stretch ratios λ_i (i = 1, 2, 3) are given as $\lambda_1 = \lambda_U$, $\lambda_2 = \lambda_3 = \lambda_U^{-\frac{1}{2}}$.

The slope of the stress-strain curve at any given stress or strain is the tangent modulus, which is calculated by taking the derivative of stress with respect to strain from Eq. (1),

$$\frac{dT_U}{d\varepsilon_U} = \sum_{i=1}^{2} \frac{2\mu_i}{\alpha_i}\left[(\alpha_i - 1)(1 + \varepsilon_U)^{\alpha_i - 2} + (0.5\alpha_i + 1)(1 + \varepsilon_U)^{-0.5\alpha_i - 2}\right] \tag{2}$$

The tangent modulus at the initial linear portion of the stress-strain curve under small deformations is Young's modulus. The Young's modulus of the TM is determined by linear regression of the tangent modulus data up to a strain of 0.25.

2.5. Inverse method

For each sample, the values of μ_i and α_i, are determined by minimizing a cost function, $C(\mu_i, \alpha_i)$ with respect to μ_i and α_i. The cost function is defined such that a minimal value achieves when the volume displacements calculated using the FEM model for a particular sample matches the corresponding values measured from the experiment:

$$C = \sum_{i=1}^{M} (\Delta V_i^{exp} - \Delta V_i^{FEM})^2 \tag{3}$$

where ΔV_i^{exp} is the volume displacement obtained in experiment under a given pressure, ΔV_i^{FEM} is the corresponding FEM simulated volume displacement, M is the number of pressurized states.

In the iterative solving process, the values of μ_i and α_i are first set to be identical to the parameters for a human TM (Cheng et al., 2007). Uniform pressures in the range of 0 kPa–1.0 kPa with an increment of 0.125 kPa are applied on the medial side and the lateral side, corresponding to the pressure used in the experiments. The volume displacement under each static pressure is calculated by summing the volume displacements of all the elements. An iterative procedure is used to modify μ_i and α_i until the volume displacements calculated by the FEM model match well with the corresponding experimental data, similar to the procedure documented in our previous work (Liang et al., 2015).

3. Results

3.1. Surface topography

A typical reconstruction of the human TM in Fig. 5 shows the surface height topography of the TM under 0 kPa, +1.0 kPa and −1.0 kPa

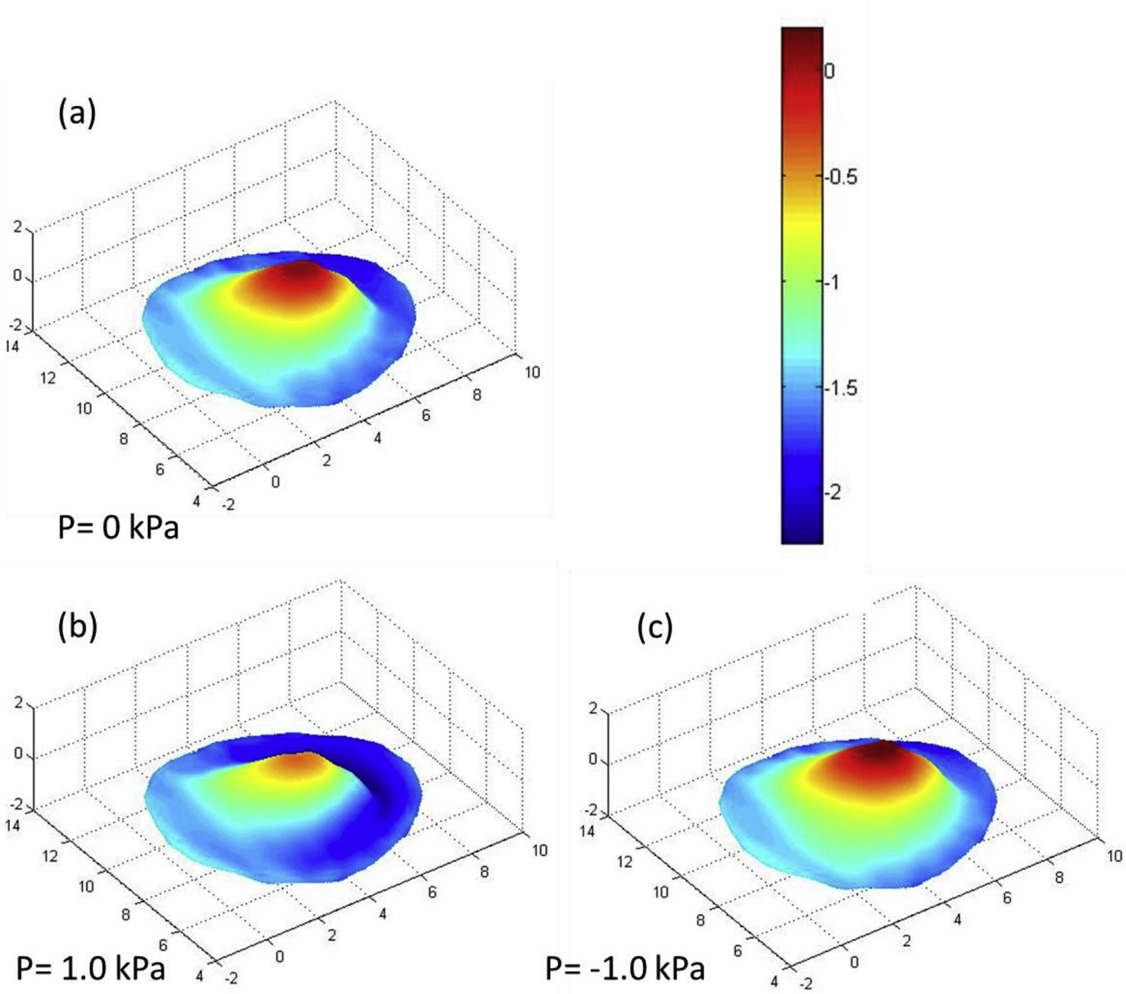

Fig. 5. Typical 3D reconstructed tomogram of a human TM surface (TB16-19). The unit in the figure is mm.

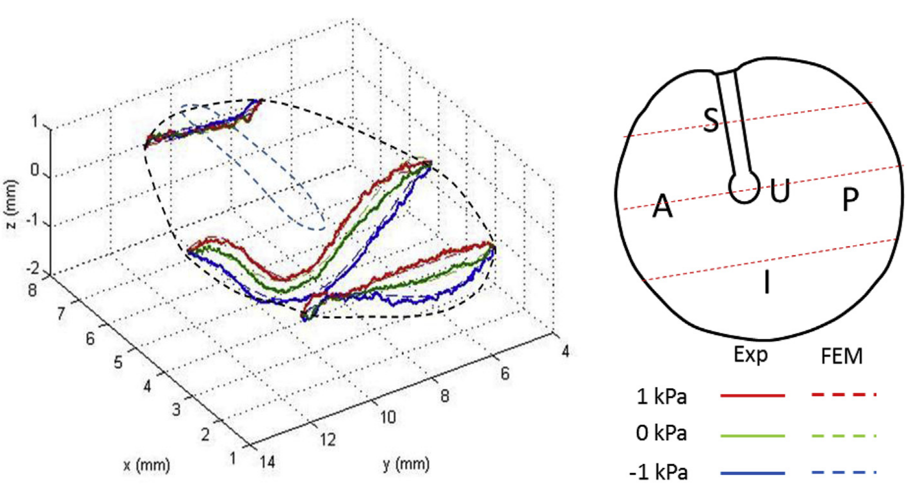

Fig. 6. Comparison of the surface profile of a typical TM between experimental (Exp) results and FEM simulation under −1.0 kPa, 0 kPa and +1.0 kPa pressures. The three dash-dot lines along the anterior-posterior direction in the schematic in the right figure show the cross-sections for comparison in the figure on the left. The labels in the schematics are: A (anterior quadrant), P (posterior quadrant), S (superior quadrant), I (inferior quadrant), and U (umbo).

pressures. For the purpose of validation, the height topographic profile of a typical human TM sample is compared between experiment and simulation in three cross-sections at each of the three different pressure levels (−1.0 kPa, 0 kPa and +1.0 kPa) (Fig. 6). Simulation height profiles are reasonably close to the experimental results, with errors less than 10%.

Fig. 7 shows the contour of displacement along the z-direction perpendicular to the imaging plane of the TM, obtained by subtracting the surface profile at 0 kPa pressure from the corresponding profiles at ± 1.0 kPa pressure. Although the magnitudes of the displacement are different under the application of positive and negative pressures, the profile of the displacement distribution is generally similar between them. The displacement is close to zero at the superior and gradually increases along the superior-inferior direction and along the radial direction from the manubrium. The maximum displacement is found in the inferior area, forming a U-shape plateau surrounding the umbo at

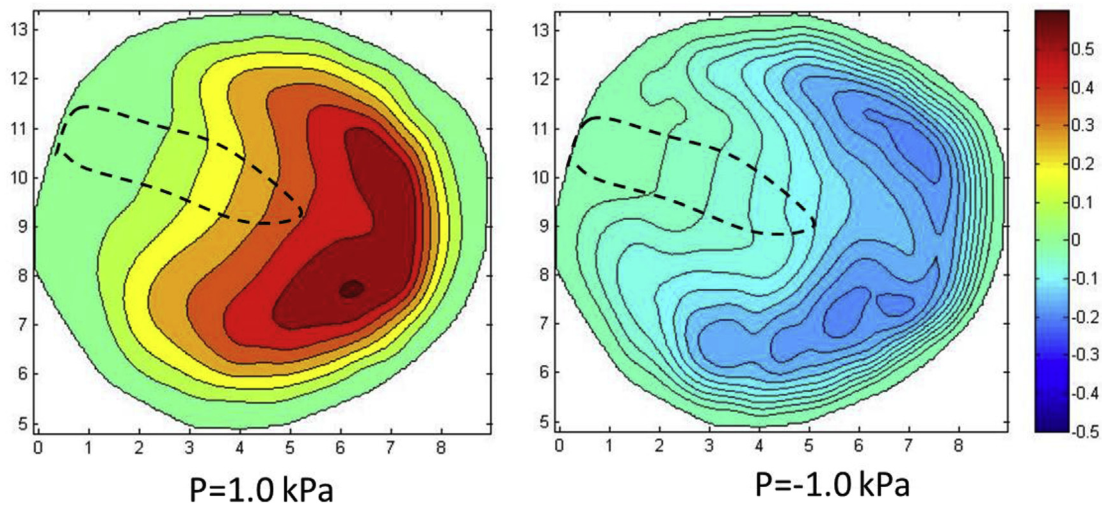

Fig. 7. Displacement maps calculated from the data in Fig. 6. The dash line shows the boundary of the manubrium. The step distance between the height line is 0.05 mm.

approximately midway between the malleus and the annulus ring under both positive and negative pressure cases. In the case of negative pressure, the area with the peak displacement is separated into two sections between the anterior and posterior. This could be caused by the uneven distribution of the thickness of the human TM along the radial direction from the malleus to the edge of the annulus ring. The deformation pattern is in general similar to what is seen for cat, guinea pig, and chinchilla TMs due to the similarity of the geometries of the TMs in these species (Liang et al., 2015, 2016; Ladak et al., 2004) and is consistent with what has been reported on the human TMs (Dirckx and Decraemer, 1991).

3.2. Volume displacement-pressure relationship

The volume displacements are plotted against the pressure for both control and post-blast TMs as shown in Fig. 8. It is noted that, for soft tissues such as TM, the volume displacement-pressure relationship depends highly on the state of the loading or unloading. When pre-conditioning is conducted, the hysteresis of the TM samples is reduced to a negligible level. Therefore the volume displacements are only computed under the loading stage in this study. The curves shown in Fig. 8 are in general asymmetric with respect to the point at zero-pressure and zero-volume displacement. For the control TMs, the average volume displacement under positive pressure is about 40% higher than the corresponding value under negative pressure with the same magnitude. For post-blast TMs, the average volume displacement under a positive pressure is also higher, about 25% higher than the corresponding values under a negative pressure of the same magnitude. This asymmetry of the deformation of the TM is due to its nearly conical geometry. The fact that the manubrium structure crosses the apex of the TM also contributes to its uneven deformation under positive and negative pressure. The malleus on the medial side of the TM is held in tension with ossicular chains connecting to it, which reduces the TM deformation as pressure increases in the negative direction (Kartush et al., 2006). The asymmetrical volume displacement is consistent with our previous findings (Liang et al., 2016) and others' findings on TMs of mammals such as gerbils (Gea et al., 2010), cats (Funnell and Decraemer, 1996), and humans (Gaihede et al., 2007).

3.3. Mechanical properties of control and post-blast TMs

Tables 1 and 2 list the dimensions and the material property parameters in the Ogden model for each TM. The model parameters are determined from the entire loading cycle for each TM sample. The stress-strain relationships of the control and post-blast TMs determined using Eqn. (1) and the parameters in Tables 1 and 2 are plotted in Fig. 9. The curves shown in Fig. 9 demonstrate hyperelastic behavior of the human TM: the TM becomes stiffer as the strain increases. In Fig. 10, the tangent modulus is also plotted against the uniaxial strain. The nonlinearity of the tangent modulus is easier to observe: as the strain increases, the tangent modulus decreases at strains below 20%, and it then gradually increases at strains above 20%. At a strain near zero, the tangent modulus is 8.5 MPa for the control TMs and 6.7 MPa for the post-blast TMs. At 30% strain, which is the maximum strain on the TM determined by FEM analysis, the tangent modulus is slightly lower: 7.5 MPa for the control TM and 6.1 MPa for the post-blast TM. The average Young's modulus is calculated based on the results obtained from 8 TMs using Eqn. (2). In this study, the average tangent modulus, at strains less than 25%, is defined as the representative Young's modulus for comparison. The average values of Young's modulus for the control TMs and post-blast TMs are ~7.8 MPa and ~6.3 MPa respectively. The average Young's modulus of the control TMs is lower than that measured by Luo et al. using split Hopkinson tension bar (Luo et al., 2016) and higher than that measured by Rohani et al. using a pressurization method (Rohani et al., 2017). This is probably because of the difference in the measurement methods applied.

4. Discussion

The TM is a complex tissue that consists of an epidermis layer, a connective layer (lamina propria), and a mucosal epithelial layer (Lim, 1995). The core of the structural layer, the lamina propria, is a fibrous layer made up of outer radial fibers and inner circular (circumferential) fibers in addition to parabolic fibers. The fracture strength of the radial fibrous layer is higher than that of the circumferential fibrous layer. On exposure to blast waves, the TM is prone to break in the circumferential direction rather than in the radial direction. To evaluate the effect of blast wave on the microstructures of the TM, a post-blast TM sample is observed with scanning electronic microscopy (SEM) and compared with an SEM image of a control TM (Fig. 11). In this study the intensity of the blast wave used is not enough to induce perforation across the entire TM thickness, it has induced damage on the TM as micro-ruptures in the fibrous layer. In contrast to the well-aligned circumferential fibers in the control TM, some fibers are randomly aligned over the circumferential fibrous layer of the post-blast TM. It is noticed that, although it is beneficial to investigate the radial fibrous layers further by removing or dissecting the circumferential layer, such a process can induce secondary damage to the radial fibrous layers. Thus, we are

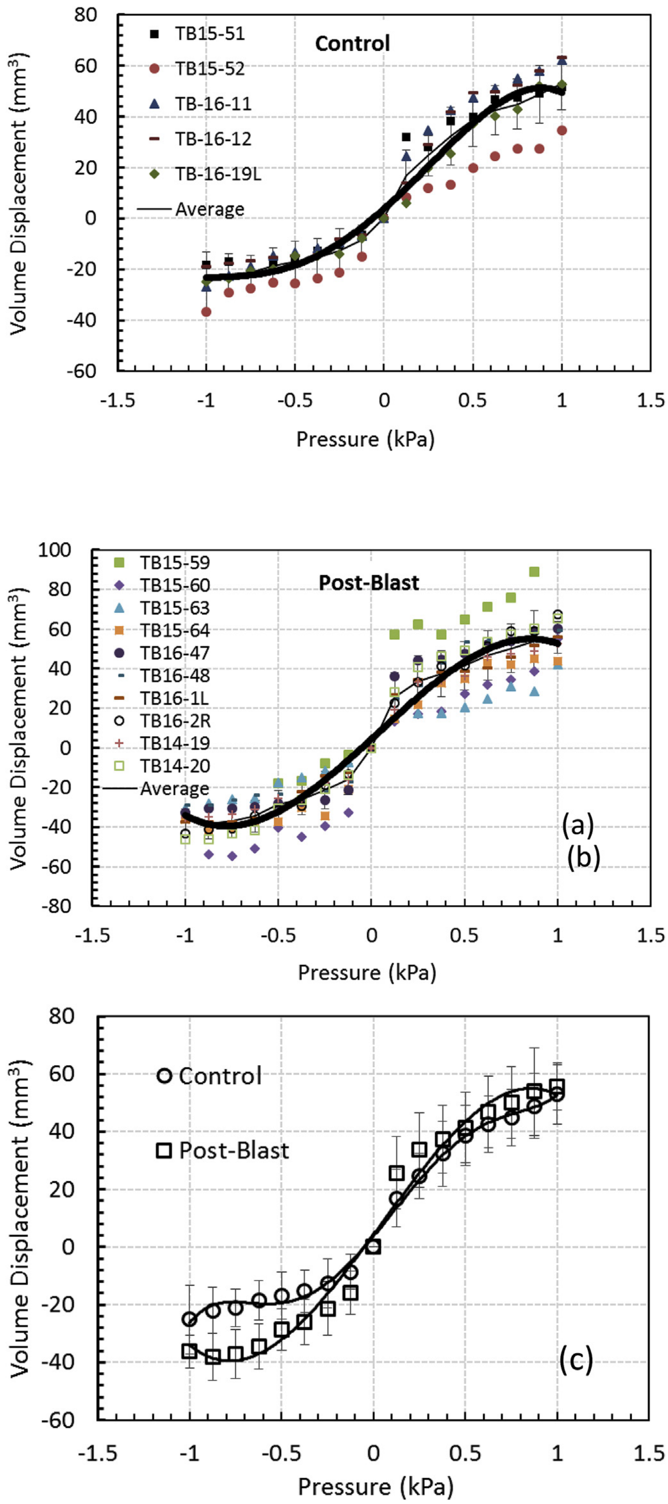

Fig. 8. Volume displacement – pressure relationships for control (n = 5) shown in (a) and post-blast human (n = 16) TM shown in (b). Comparison between the two groups of TMs is also plotted with the standard deviation as the error bar shown in (c).

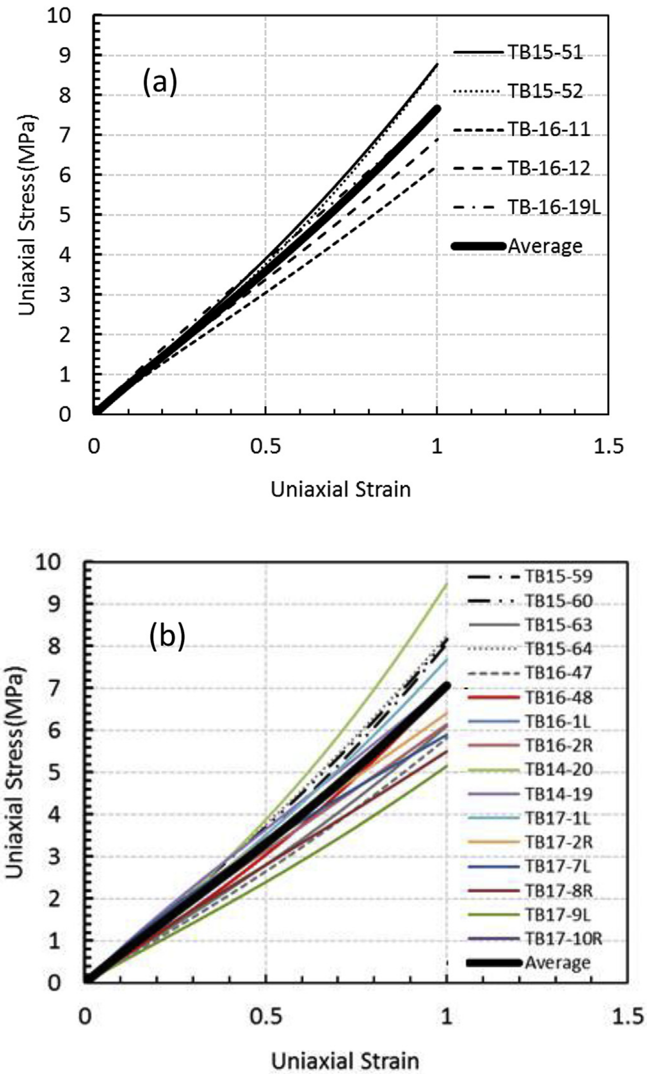

Fig. 9. Stress-strain relationships for the control (n = 5) shown in (a) and post-blast (n = 16) human TMs shown in (b).

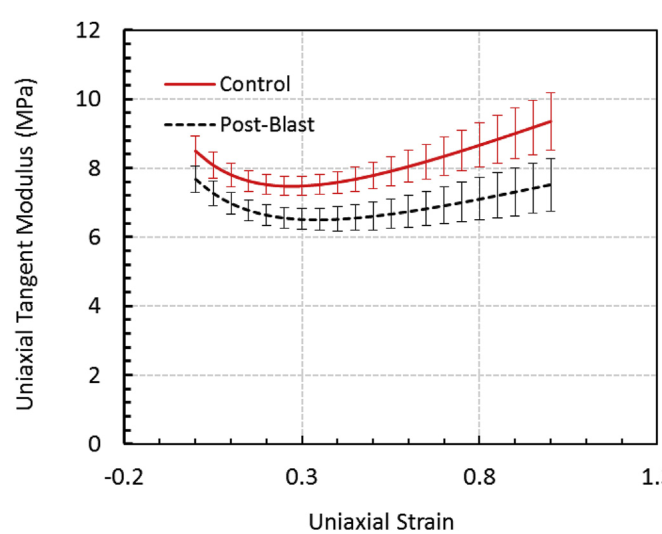

Fig. 10. Comparison of tangential modulus data for control (n = 5) and post-blast groups (n = 16). The error bars show the standard deviation.

unable to observe the blast damage to the radial fibers using SEM. The damage in the post-blast TM is likely responsible for the reduction of mechanical properties in comparison with the control TM.

From Figs. 8 and 10, it is seen that the mechanical properties of the human TM changed after the TM is exposed to the blast overpressure. In the volume displacement-pressure relationship, the alternation of the

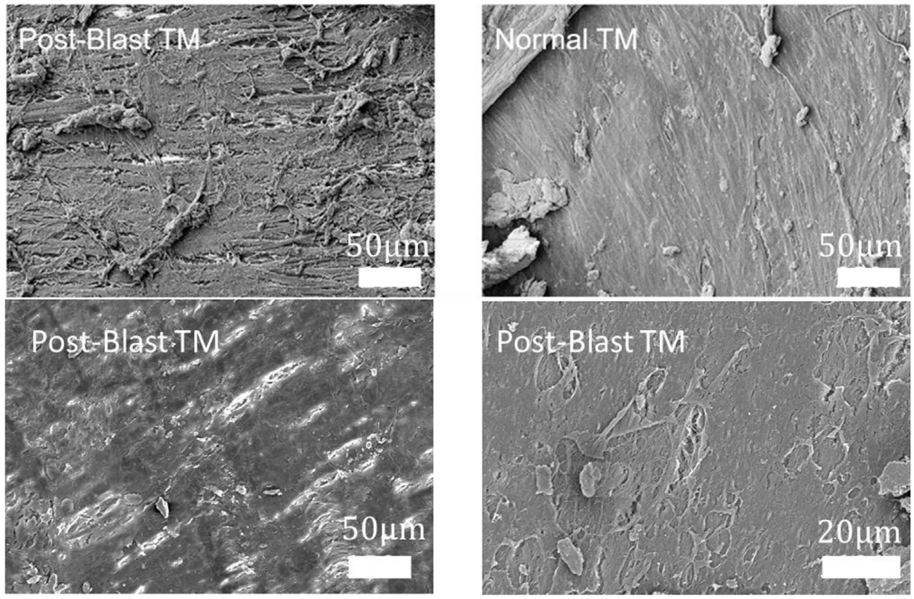

Fig. 11. Typical SEM micrographs for post-blast and control human TMs.

mechanical response exhibits asymmetry between positive pressure and negative pressure. In the positive direction, the volume displacement of the post-blast TM is nearly identical to that of the control TM. This is different from the observation of chinchilla TM (Liang et al., 2016). This could be due to the different ways of sample preparation for the fringe projection measurement. For the chinchilla, the entire cochlea and the stapes were removed and the positive pressure was applied from the lateral side of the TM, therefore the TM did not have constraint for motion under both the positive and negative pressure. The ruptures can form and propagate in both directions. For the human TM samples used in this work, the entire cochlea and the ossicular chain are kept intact and the positive pressure is applied from the medial side of the TM. When a positive pressure is applied to the human TM, the ossicular chain is stretched and restricts the deformation from distorting the conical geometry of the TM, thus the ruptures cannot propagate along this direction. As a result, the volume displacement in the positive direction does not show a significant increase as in the case under negative pressure.

The tangent modulus of the TM, however, which is independent of the structure of the system, shows clearly the weakening of the TM after its exposure to blast overpressure. The Young's modulus, which is identical to the linear section of the tangent modulus, decreases by about 20%. This reduction is much lower than the 50% reduction in Young's modulus for the chinchilla TM in our previous work (Liang et al., 2017). It is reasoned that the thickness of the human TM plays an important role to mitigate the damage in comparison with the thinner TM of the chinchilla: the thickness of the human TM is about 80 μm, while it is 20 μm for a chinchilla TM. The value of the reduction in Young's modulus in this study is consistent with what is reported in the work of Luo et al. (2016). In that study, it is found that at a low strain rate, the TM exhibits 22% reduction in Young's modulus in the radial direction and about 8% reduction in the modulus in the circumferential direction. Although it is still unable to quantify the damage induced by the sample preparation of cutting the TM into strips, the comparison between our data and Luo's data implies that the fibers in the radial direction dominate the performance of the TM at least at low strain rates. The reduction of the stiffness in the intact TM is smaller than what is reported by Engles et al. on post-blast human TM strips (2017). In that study, the storage modulus of the post-blast human TMs exhibits a reduction of more than 50% in comparison with that of control TMs. The reason for such a large magnitude in the change of storage modulus is still unclear. One possible reason is that the small transverse vibration loading is applied to the TM strip. Such a loading condition is different from what is used in our work.

In this work, the micro-fringe projection technique allows investigation of the blast damage on the TM without dissecting the TM sample. This approach eliminates the effect of possible damage and alteration of collagen fibers in the preparation of strip specimens. The direct measurement of the mechanical properties of a human TM rather than a chinchilla TM eliminates the need to factor the species difference between human and chinchilla. However, this method depends on the ability to apply pressure to the confined middle ear, consequently this technique cannot be applied for a ruptured TM. In addition, in the calculation of the mechanical properties using the inverse method, the TM is considered as an isotropic and homogenous material. Thus, the mechanical properties reported herein represent the overall effective isotropic properties and cannot identify the potentially extremely localized damage. This study provides results on the change of the effective mechanical property the TM under overpressure, which can be used in FEM simulations to evaluate the effect of TM damage on the sound transmission in the middle ear. In the work in the future, orthotropic and inhomogeneous characteristics of the TM need to be considered so that a realistic model of the blast-damaged TM model can be established.

The results obtained in this work indicates that repetitively exposed to low pressure level blast induces mechanical damages to the TM. However, the threshold of the overpressure inducing microstructural damage was not determined; in addition, how the damage is accumulated and when a cumulative damage reaches a detrimental level on the TM were not determined. These are areas that require further investigation.

5. Conclusion

The effect of blast overpressure on the mechanical property change of the TM in humans is evaluated using a micro-fringe projection system with pressure loading applied on the entire TM suspended on an annulus. FEM models for human TMs are developed to determine the mechanical properties of the TMs. It is shown that the Young's modulus of the post-blast human TMs decreased by about 20% in comparison with control TMs. The measurement technique used in this work is in-situ and does not induce potential damage to the TM in preparation.

The technique thus allows a more accurate evaluation of the blast effect on the human TM mechanical properties change.

Acknowledgement

We acknowledge the support of DOD W81XWH-13-MOMJPC5-IPPEHA, NSF CMMI-1636306, CMMI-1661246 and CMMI-1726435. We thank Mr. Warren Engles for the SEM imaging and Mr. Don U. Nakmali for preparation of TM samples. Lu acknowledges the Luis A. Beecherl Jr. endowed chair for additional support.

References

Aernouts, J., Soons, J.A.M., Dirckx, J.J.J., 2010. Quantification of tympanic membrane elasticity parameters from in situ point indentation measurements: validation and preliminary study. Hear. Res. 263 (1–2), 177–182.
Cheng, T., Dai, C.K., Gan, R.Z., 2007. Viscoelastic properties of human tympanic membrane. Ann. Biomed. Eng. 35 (2), 305–314.
De Greef, D., Goyens, J., Pintelon, I., Bogers, J.P., Van Rompaey, V., Hamans, E., Van de Heyning, P., Dirckx, J.J.J., 2016. On the connection between the tympanic membrane and the malleus. Hear. Res. 340, 50–59.
Dirckx, J.J., Decraemer, W.F., 1991. Human tympanic membrane deformation under static pressure. Hear. Res. 51 (1), 93–105.
Dirckx, J.J.J., Decraemer, W.F., 1997. Coating techniques in optical interferometric metrology. Appl. Opt. 36 (13), 2776–2782.
Dougherty, A.L., MacGregor, A.J., Han, P.P., Viirre, E., Heltemes, K.J., Galarneau, M.R., 2013. Blast-related ear injuries among U.S. military personnel. J. Rehabil. Res. Dev. 50 (6), 893–904.
Engles, W.G., Wang, X., Gan, R.Z., 2017. Dynamic properties of human tympanic membrane after exposure to blast waves. Ann. Biomed. Eng. 45 (10), 2383–2394.
Funnell, W.R.J., Decraemer, W.F., 1996. On the incorporation of moire shape measurements in finite-element models of the cat eardrum. J. Acoust. Soc. Am. 100 (2), 925–932.
Gaihede, M., 1996. Tympanometric preconditioning of the tympanic membrane. Hear. Res. 102 (1–2), 28–34.
Gaihede, M., Liao, D.H., Gregersen, H., 2007. In vivo areal modulus of elasticity estimation of the human tympanic membrane system: modelling of middle ear mechanical function in normal young and aged ears. Phys. Med. Biol. 52 (3), 803–814.
Gan, R.Z., Leckness, K., Nakmali, D., Ji, X.D., 2018. Biomechanical measurement and modeling of human eardrum injury in relation to blast wave direction. Mil. Med. 183 (1), 245–251.
Gea, S.L.R., Decraemer, W.F., Funnell, W.R.J., Dirckx, J.J.J., Maier, H., 2010. Tympanic membrane boundary deformations derived from static displacements observed with computerized tomography in human and gerbil (vol 11, pg 1, 2010). JARO J. Assoc. Res. Otolaryngol. 11 (3) 525-525.
Kartush, J.M., Babu, S.C., 2006. "Ossicular Chain Reconstruction: Maximizing Success and Minimizing Errors," Ear and Temporal Bone Surgery. In: Wiet, R.J. (Ed.), Thieme Clinical Collections, pp. 90–92.
Ladak, H.M., Decraemer, W.F., Dirckx, J.J., Funnell, W.R., 2004. Response of the cat eardrum to static pressures: mobile versus immobile malleus. J. Acoust. Soc. Am. 116 (5), 3008–3021.
Liang, J., 2009. Determination of the Mechanical Properties of guinea Pig Tympanic Membrane Using Combined Fringe Projection and Simulations. Oklahoma State University.
Liang, J., Fu, B., Luo, H., Nakmali, D., Gan, R.Z., Lu, H., 2015. Characterization the nonlinear elastic behavior of Guinea pig tympanic membrane using micro-fringe projection. Int. J. Exp. Comput. Biomech. 3, 319–344.
Liang, J.F., Luo, H.Y., Yokell, Z., Nakmali, D.U., Gan, R.Z., Lu, H.B., 2016. Characterization of the nonlinear elastic behavior of chinchilla tympanic membrane using micro-fringe projection. Hear. Res. 339, 1–11.
Liang, J., Yokell, Z.A., Nakmaili, D.U., Gan, R.Z., Lu, H., 2017. The effect of blast overpressure on the mechanical properties of a chinchilla tympanic membrane. Hear. Res. 354, 48–55.
Lim, D.J., 1995. Structure and function of the tympanic membrane: a review. Acta Oto-Rhino-Laryngol. Belg. 49 (2), 101–115.
Luo, H., Dai, C., Gan, R.Z., Lu, H., 2009. Measurement of young's modulus of human tympanic membrane at high strain rates. J. Biomech. Eng. 131 (6), 064501.
Luo, H., Jiang, S., Nakmali, D.U., Gan, R.Z., Lu, H., 2016. Mechanical properties of a human eardrum at high strain rates after exposure to blast waves. J. Dyn. Behav. Mater. 2, 59–73.
Mathews, Z.R., Koyfman, A., 2015. Blast injuries. J. Emerg. Med. 49 (4), 573–587.
Nakagawa, A., Manley, G.T., Gean, A.D., Ohtani, K., Armonda, R., Tsukamoto, A., Yamamoto, H., Takayama, K., Tominaga, T., 2011. Mechanisms of primary blast-induced traumatic brain injury: insights from shock-wave research. J. Neurotrauma 28 (6), 1101–1119.
O'Connor, K.N., Tam, M., Blevins, N.H., Puria, S., 2008. Tympanic membrane collagen fibers: a key to high-frequency sound conduction. The Laryngoscope 118 (3), 483–490.
Ortiz, M.H., Patterson, E.A., 2005. Location and shape measurement using a portable fringe projection system. Exp. Mech. 45 (3), 197–204.
Owens, B.D., Kragh, J.F., Wenke, J.C., Macaitis, J., Wade, C.E., Holcomb, J.B., 2008. Combat wounds in operation Iraqi freedom and operation enduring freedom. J. Trauma 64 (2), 295–299.
Remenschneider, A.K., Lookabaugh, S., Aliphas, A., Brodsky, J.R., Devaiah, A.K., Dagher, W., Grundfast, K.M., Heman-Ackah, S.E., Rubin, S., Sillman, J., Tsai, A.C., Vecchiotti, M., Kujawa, S.G., Lee, D.J., Quesnel, A.M., 2014. Otologic outcomes after blast injury: the Boston marathon experience. Otol. Neurotol. 35 (10), 1825–1834.
Rohani, S.A., Ghomashchi, S., Agrawal, S.K., Ladak, H.M., 2017. Estimation of the Young's modulus of the human pars tensa using in-situ pressurization and inverse finite-element analysis. Hear. Res. 345, 69–78.
Wang, B., Lu, H.B., Kim, G.H., 2002. A damage model for the fatigue life of elastomeric materials. Mech. Mater. 34 (8), 475–483.
Wolf, S.J., Bebarta, V.S., Bonnett, C.J., Pons, P.T., Cantrill, S.V., 2009. Blast injuries. Lancet 374 (9687), 405–415.
Yeh, D.D., Schecter, W.P., 2012. Primary blast injuries-an updated concise review. World J. Surg. 36 (5), 966–972.